Supplemental Materials

Methods

Tissue culture transfection

SOD1 mutants have been previously characterized (Wang et al. 2003). αB-crystallin cDNA (Clontech, Mountain View, CA, USA) was expressed in the pEF-BOS vector (Mizushima and Nagata 1990). GFP cDNA (Clontech, Mountain View ,CA, USA) was expressed in the pcDNA3.1(A)-Myc vector (Invitrogen, Carlsbad, CA, USA). Transient transfection was performed in HEK293-FT cells as previously described (Wang et al. 2003;Karch and Borchelt 2008).

SOD1 aggregation assay by differential extraction

The procedures used to assess SOD1 aggregation by differential detergent extraction and centrifugation in spinal cords and muscle were similar to previous descriptions (Wang et al. 2003;Karch and Borchelt 2008). Protein concentration was measured in the detergent-insoluble and detergent-soluble fractions by BCA method as described by the manufacturer (Pierce, Rockford, IL, USA).

Immunoblotting and quantitative analysis

Standard sodium dodecyl sulfate-polyacrylamide gel electrophoresis (SDS-PAGE) was performed in 18% Tris-Glycine gels (Invitrogen, Carlsbad, CA, USA). Samples were boiled for 5 minutes in Laemmli sample buffer prior to electrophoresis (Laemmli 1970). The antibodies used to probe immunoblots are listed in Supplemental Table 1.

Quantification of SOD1 protein in insoluble and soluble fractions was performed by measuring the band intensity of SOD1 in each lane using a Fuji imaging system (FUJIFILM, LifeScience, Stamford, CT, USA) as described previously (Karch and Borchelt 2008). The ratio of the band intensity for insoluble to soluble SOD1 was calculated for each transfection experiment. Averages for data from multiple experiments and the standard error of the mean (SEM) was calculated for aggregation ratio of each sample in each experiment. Statistical significance was measured using an unpaired, 2-tailed, t-test.

Histology

After inducing deep anesthesia, mice were transcardially perfused with cold PBS and then 4% paraformaldehyde in 1x PBS. After 48 hours of post-fixation, tissues were transferred to 30% sucrose for at least 48 hours prior to cryostat sectioning (Microm HM550). Coronal sections of spinal cord (14 microns) were cut and stored in anti-freeze solution (100 mM sodium acetate, 250 mM polyvinyl pyrolidone, 40% ethylene glycol, pH 6) and stored at -20°C. To stain tissue, sections were washed in PBS prior to blocking in 5% normal goat serum (Invitrogen, Calsbad, CA). Sections were then incubated in primary and secondary antibodies with PBS, 5% normal goat serum, and 1% triton. Tissue was stained with antibodies listed in Supplemental Table 1. Images were captured using an Olympus IX81-DSU Spinning Disk confocal microscope.

Levels of αB-crystallin in Gn.G37R, Gn.L126Z, and PrP.G37R mice

In all three lines of fALS mice, αB-crystallin was predominantly detected in the detergent-insoluble fraction whether wild-type (+/+) or reduced (+/-) levels of αB-crystallin were present in the tissue (Suppl. Fig. 6A, lanes 3-4, 6-7, 9-10). Only when both αB-crystallin alleles were present was αB-crystallin detected in the detergent-soluble fraction (Suppl. Fig. 6B, lanes 3,6,9). The levels of insoluble αB-crystallin in spinal cords of symptomatic Gn.G37R mice were much higher than that of symptomatic Gn.L126Z mice (Suppl. Fig. 6A, lanes 3,4). By immunohistochemical examination, we observed punctate reactivities with αB-crystallin antibodies in spinal cords of symptomatic GnG37R mice (Suppl. Fig. 7A & B) that were absent in mutant mice lacking αB-crystallin (Suppl. Fig. 7C). The pattern of αB-crystallin reactivity in non-symptomatic PrP.G37R mice (Suppl. Fig. 7D & E) resembled that of normal mice expressing the normal level of αB-crystallin (Suppl. Fig. 7J). In normal mice, the cells that seem to accumulate αB-crystallin have morphologies of oligodendrocytes (Wang et al. 2005;Wang et al. 2008). In symptomatic Gn.L126Z mice, which seem to have a very weak upregulation of αB-crystallin, we noted a robust immunoreactivity for αB-crystallin in cells of astrocyte morphology (Suppl. Fig. 7G). Thus, in this side-by-side comparison of different fALS mice, we find that Gn.L126Z mice differ from other mutants in regards to the magnitude of αB-crystallin induction and the types of cells that seem to accumulate the chaperone.

Accumulation of SOD1 immunoreactivity in mutant SOD1 mice lacking αB-crystallin

To examine possible changes in the types of neural cells that accumulate misfolded SOD1 when αB-crystallin levels were reduced (+/-) or eliminated (-/-), spinal cords from each variant were fixed, and frozen sections were stained using cell-type specific markers. In this study, we used an antiserum (hSOD1 antibody) that recognizes a peptide from amino acids 24-36 that is unique to human SOD1 (Bruijn et al. 1997). To determine if this antibody is able to recognize normally folded SOD1, we immunoprecipitated purified wild-type SOD1 protein (made by D. Winkler in the laboratory of Dr. P. John Hart, University of Texas Health Science Center at San Antonio) with the hSOD1 antibody (Suppl. Fig 8). We found that the purified wild-type SOD1 protein could only be captured with the hSOD1 antibody when the protein was denatured (Suppl. Fig 8). Thus, it is likely that this antibody recognizes protein that is not in its native state. Using this antibody, we sought to determine whether the general pattern of SOD1 immunoreactivity differed between mice that express wild-type levels of αB-crystallin and mice that express reduced or no αB-crystallin. To identify cell types within these tissues, we used standard cell markers (GFAP and NeuN) to identify astrocytes and neurons, respectively.

In Gn.L126Z (Suppl. Fig. 9, panels A-R) and Gn.G37R mice (Suppl. Fig. 10, panels A-X), among the different αB-crystallin genotypes (+/+, +/-, -/-), we observed no unique pattern of SOD1 immunoreactivity that could be associated with loss of αB-crystallin. SOD1 immunoreactivity was most prominent in motor neurons, with little or

no observable reactivity in astrocytes. In general, in both Gn.G37R and Gn.L126Z mice, astrocytes appeared to surround SOD1 positive motor neurons (Suppl. Fig 9 and 10, panels A-C, G-I, M-O). Cells exhibiting SOD1 immunoreactivity were positive for the neuronal marker NeuN (Suppl. Fig. 9 and 10, panels D-F, J-L, P-R). Thus, when αB-crystallin is reduced (+/-) or eliminated (-/-), there were no obvious changes in the location of SOD1 immunoreactivity compared with SOD1 transgenic mice expressing wild-type levels of αB-crystallin.

Reference List

Bruijn L. I., Becher M. W., Lee M. K., Anderson K. L., Jenkins N. A., Copeland N. G., Sisodia S. S., Rothstein J. D., Borchelt D. R., Price D. L., and Cleveland D. W. (1997) ALS-linked SOD1 mutant G85R mediates damage to astrocytes and promotes rapidly progressive disease with SOD1-containing inclusions. *Neuron* **18,** 327-338.

Karch C. M. and Borchelt D. R. (2008) A limited role for disulfide cross-linking in the aggregation of mutant SOD1 linked to familial amyotrophic lateral sclerosis. *J Biol Chem* **283,** 13528-13537.

Laemmli U. K. (1970) Cleavage of structural proteins during the assembly of the head of bacteriophage T4. *Nature (London)* **227,** 680-685.

Mizushima S. and Nagata S. (1990) pEF-BOS, a powerful mammalian expression vector. *Nucleic Acids Res* **18,** 5322.

Wang J., Martin E., Gonzales V., Borchelt D. R., and Lee M. K. (2008) Differential regulation of small heat shock proteins in transgenic mouse models of neurodegenerative diseases. *Neurobiol Aging* **29,** 586-597.

Wang J., Slunt H., Gonzales V., Fromholt D., Coonfield M., Copeland N. G., Jenkins N. A., and Borchelt D. R. (2003) Copper-binding-site-null SOD1 causes ALS in transgenic mice: aggregates of non-native SOD1 delineate a common feature. *Hum Mol Genet* **12,** 2753-2764.

Wang J., Xu G., Li H., Gonzales V., Fromholt D., Karch C., Copeland N. G., Jenkins N. A., and Borchelt D. R. (2005) Somatodendritic accumulation of misfolded SOD1-L126Z in motor neurons mediates degeneration: {alpha}B-crystallin modulates aggregation. *Hum Mol Genet* **14,** 2335-2347.

Supplemental Figure Legends

Suppl. Figure S1: Expression of αB-crystallin in cells transfected with SOD1 and αB-crystallin expression vectors. Detergent-insoluble protein fractions and detergent-soluble protein fractions from Figure 1 were electrophoresed in 18% Tris-Glycine gels and immunoblotted with αB-crystallin antiserum. A. Detergent-insoluble (20 μg). B. Detergent-soluble (5 μg).

Suppl. Figure S2: Hsp70 and Hsp40 are constitutively and highly induced in HEK293-FT cells. Cells were not exposed to heat shock, or heat shocked at 42°C for 30 minutes and harvested 5 h or 24 h after heat shock. Cell lysates were sonicated in PBS and electrophoresed in an 18% Tris Glycine gel. Immunoblots were probed with Hsp70 and Hsp40 antibodies. Image is representative of three repetitions of the experiment.

Suppl. Figure S3: SOD1 aggregation is restricted to the brainstem and spinal cord in Gn.L126Z mice. Organs and nervous tissues were extracted in non-ionic detergent and run on 18% Tris-Glycine gels. Immunoblots were probed with hSOD1 antiserum. A. Detergent-insoluble (20 μg). B. Detergent-soluble (5 μg).

Suppl. Figure S4: SOD1 aggregation propensity in mice expressing varying levels of αB-crystallin. The ratio of detergent-insoluble to detergent-soluble SOD1 was measured in spinal cord tissue (see Figure 4) and each measurement was graphed. °, significantly different from wild-type SOD1 ($p<0.05$). A. Gn.G37R. B. Gn.L126Z.

Suppl. Figure S5: SOD1 aggregation propensity in PrP.G37R mice expressing varying levels of αB-crystallin. The ratio of detergent-insoluble to detergent-soluble SOD1 was measured in spinal cord tissue (see Figures 4 and 5) and graphed with SEM noted by error bars.

Suppl. Figure S6: αB-crystallin is upregulated in SOD1 transgenic mice. Spinal cords were extracted in non-ionic detergent and electrophoresed in 18% Tris-Glycine gels. Immunoblots were probed with αB-crystallin antiserum. A. Detergent-insoluble (20 μg). B. Detergent-soluble (5 μg). The image shown is representative of 3 repetitions of the experiment.

Suppl. Figure S7: αB-crystallin is upregulated in astrocytes of Gn.L126Z mice. Mice were perfused with 4% paraformaldehyde and spinal cord tissue was immersed in sucrose prior to cryostat sectioning. Sections were stained with antibodies to αB-crystallin, followed by secondary fluorescent antibodies: anti-rabbit-AlexaFluor 568. Ventral horn of the spinal cord at 40x magnification. The image shown is representative of 4 repetitions of the experiment. Scale bar – 40 microns.

Suppl. Figure S8: SOD1 antibodies recognize denatured forms for SOD1. Wild-type purified protein was immunoprecipitated with hSOD1, m/hSOD1, and whole protein SOD1 antiserum in detergent (0.25% SDS, 0.5% NP40, 0.5% DOC) with or without heat denaturation. Immunoblots of antibody-SOD1 complexes captured by protein A agarose

were probed with whole protein SOD1 antiserum. A. Binding fraction (10 μl). B. Non-binding fraction (10 μl). The image shown is representative of 3 repetitions of the experiment.

Suppl. Figure S9: In Gn.L126Z mice, elimination of αB-crystallin does not alter localization of SOD1 accumulation. Mice were perfused with 4% paraformaldehyde and spinal cord tissue was immersed in sucrose prior to cryostat sectioning. Sections were stained with hSOD1 antiserum (A, D, G, J, M, P) and GFAP (B, H, N) or NeuN antiserum (E, K, Q), followed by secondary fluorescent antibodies: anti-rabbit-AlexaFluor 568 (A, D, G, J, M, P,) and anti-mouse-AlexaFluor 488 (B, E, H, K, N, Q). Ventral horn. 40x magnification. The image shown is representative of 4 repetitions of the experiment. Scale bar – 40 microns.

Suppl. Figure S10: In Gn.G37R mice, αB-crystallin elimination does not alter localization of SOD1 accumulation. Mice were perfused with 4% paraformaldehyde and spinal cord tissue was immersed in sucrose prior to cryostat sectioning. Sections were stained with hSOD1 antiserum (A, D, G, J, M, P, S, V) and GFAP antiserum (B, H, N, T) or NeuN (E, K, Q, W), followed by secondary fluorescent antibodies: anti-rabbit-AlexaFluor 568 (A, D, G, J, M, P, S, V) and anti-mouse-AlexaFluor 488 (B, E, H, K, N, Q, T, W). Ventral horn. 40x magnification. The image shown is representative of 4 repetitions of the experiment. Scale bar – 40 microns.

Suppl. Fig. 1

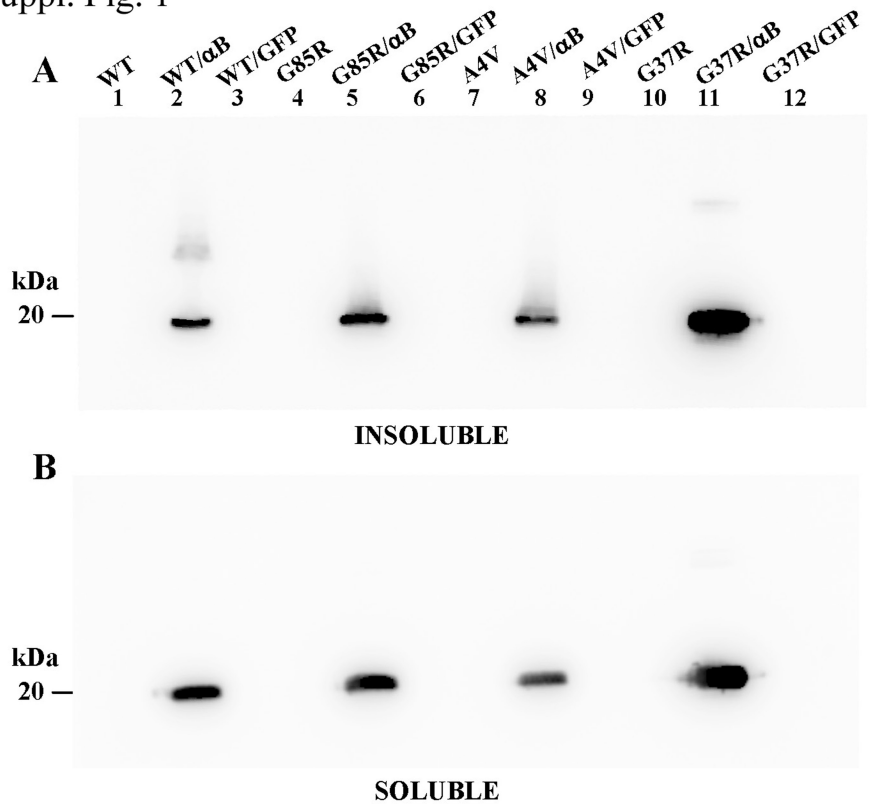
A
WT
WT/αB
WT/GFP
G85R
G85R/αB
G85R/GFP
A4V
A4V/αB
A4V/GFP
G37R
G37R/αB
G37R/GFP
1
2
3
4
5
6
7
8
9
10
11
12
kDa
20
INSOLUBLE
B
kDa
20
SOLUBLE

Suppl. Fig. 2

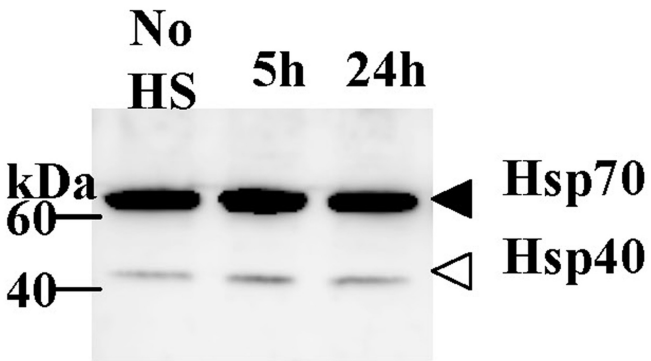

Suppl. Fig. 3

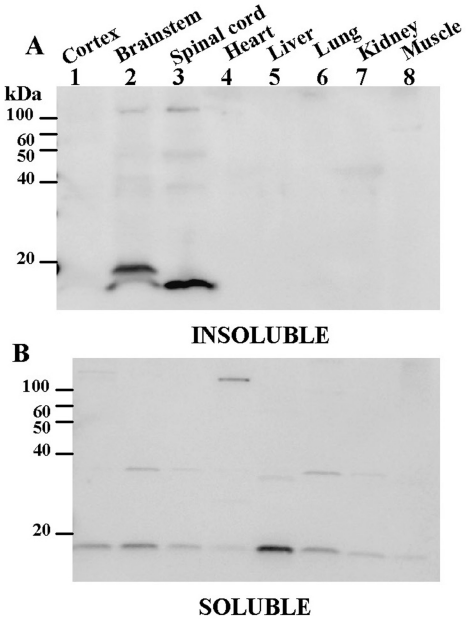
A
Cortex
Brainstem
Spinal cord
Heart
Liver
Lung
Kidney
Muscle
1 2 3 4 5 6 7 8
kDa
100
60
50
40
20
INSOLUBLE
B
100
60
50
40
20
SOLUBLE

Suppl. Fig. 4

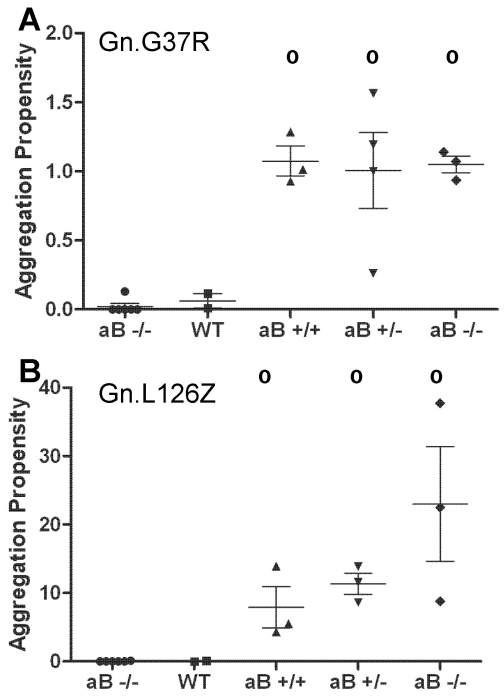
A
Gn.G37R
Aggregation Propensity
2.0
1.5
1.0
0.5
0.0
aB -/-
WT
aB +/+
aB +/-
aB -/-
B
Gn.L126Z
Aggregation Propensity
40
30
20
10
0
aB -/-
WT
aB +/+
aB +/-
aB -/-

Suppl. Fig. 5

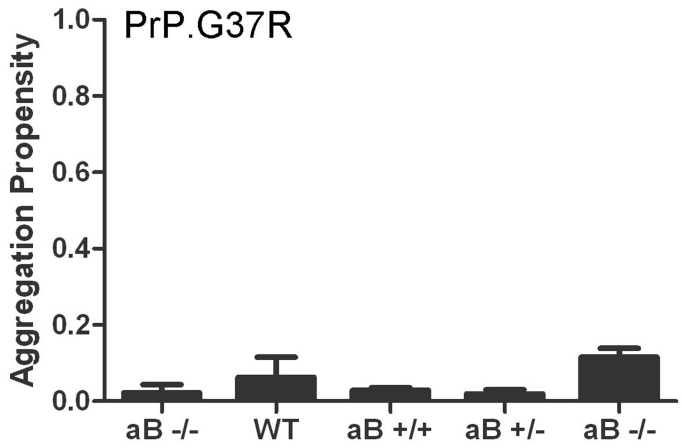
PrP.G37R
Aggregation Propensity
1.0
0.8
0.6
0.4
0.2
0.0
aB -/-
WT
aB +/+
aB +/-
aB -/-

Suppl. Fig. 6

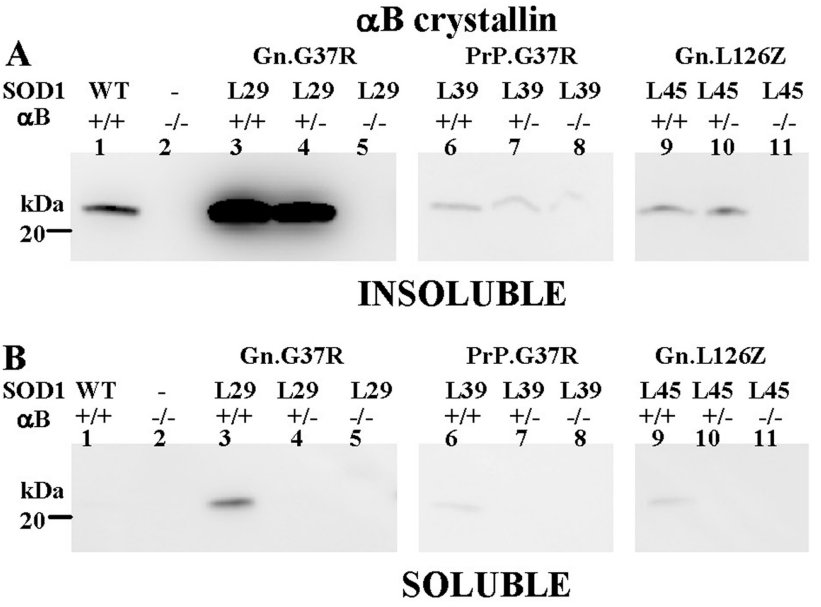
αB crystallin
A
Gn.G37R
PrP.G37R
Gn.L126Z
SOD1 WT - L29 L29 L29 L39 L39 L39 L45 L45 L45
αB +/+ -/- +/+ +/- -/- +/+ +/- -/- +/+ +/- -/-
1 2 3 4 5 6 7 8 9 10 11
kDa
20
INSOLUBLE
B
Gn.G37R
PrP.G37R
Gn.L126Z
SOD1 WT - L29 L29 L29 L39 L39 L39 L45 L45 L45
αB +/+ -/- +/+ +/- -/- +/+ +/- -/- +/+ +/- -/-
1 2 3 4 5 6 7 8 9 10 11
kDa
20
SOLUBLE

Suppl. Fig. 7

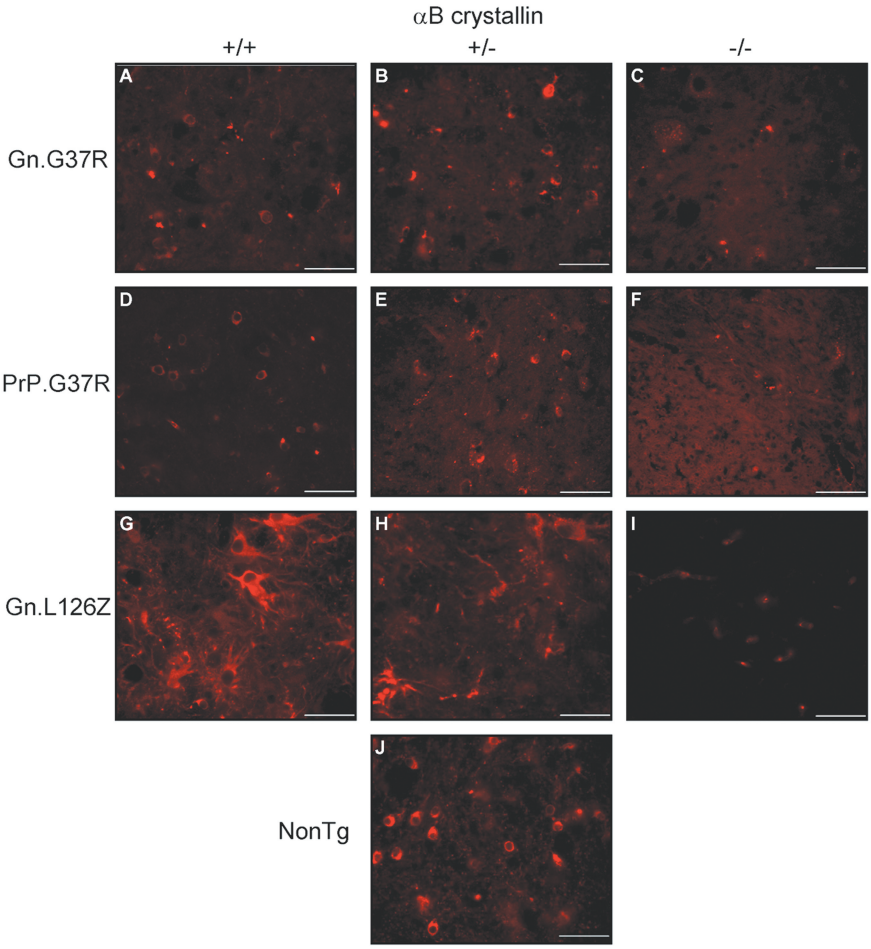

Suppl. Fig. 8

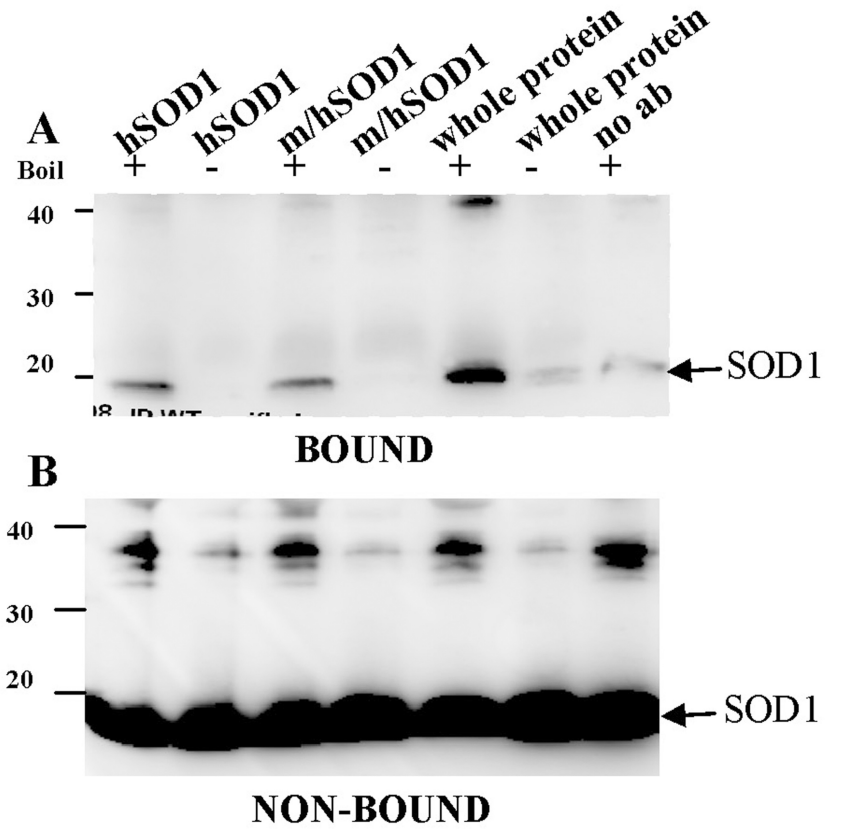
A
hSOD1
hSOD1
m/hSOD1
m/hSOD1
whole protein
whole protein
no ab
Boil
+ - + - + - +
40
30
20
SOD1
BOUND
B
40
30
20
SOD1
NON-BOUND